High-K four-quasiparticle states in ^{138}Gd

M. G. Procter,[1] D. M. Cullen,[1,*] C. Scholey,[2] P. T. Greenlees,[2] J. Hirvonen,[2] U. Jakobsson,[2] P. Jones,[2] R. Julin,[2] S. Juutinen,[2] S. Ketelhut,[2] M. Leino,[2] N. M. Lumley,[1] P. J. R. Mason,[1,†] P. Nieminen,[2] M. Nyman,[2,‡] P. Peura,[2] P. Rahkila,[2] J.-M. Regis,[3] P. Ruotsalainen,[2] J. Sarén,[2] Y. Shi,[4] J. Sorri,[2] S. Stolze,[2] J. Uusitalo,[2] and F. R. Xu[4]

[1]*Schuster Laboratory, University of Manchester, Manchester M13 9PL, United Kingdom*

[2]*Department of Physics, University of Jyväskylä, FIN-40014 Jyväskylä, Finland*

[3]*Institut für Kernphysik, Universität zu Köln, D-50937 Köln, Germany*

[4]*Department of Technical Physics, Peking University, Beijing 100871, China*

(Received 12 November 2010; revised manuscript received 8 February 2011; published 10 March 2011)

States above the known $K^\pi = 8^-$ 6 μs isomer in ^{138}Gd have been populated with the ^{106}Cd(^{36}Ar,2p2n) reaction at a beam energy of 180 MeV at the University of Jyväskylä, Finland. The recoil-isomer tagging technique was utilized to correlate delayed γ-ray decays, detected in the GREAT focal plane spectrometer, with prompt decays measured in the JUROGAM II spectrometer at the target position. The lifetime of the $K^\pi = 8^-$ isomeric state has been remeasured as 6.2(2) μs. Two high-lying strongly coupled bands have been established with $K^\pi \geqslant 12^-$. Potential-energy surface calculations, in conjunction with g factor measurements, reveal that they are built upon four-quasiparticle structures comprising two-quasineutron plus two-quasiproton configurations. The short half-life or lack of hindrance for the decays from these four-quasiparticle band-head states is reasoned to be a consequence of increased triaxial deformation and mixing due to the high density of states relative to the lower two-quasiparticle 6-μs isomeric state.

DOI: 10.1103/PhysRevC.83.034311 PACS number(s): 21.10.Re, 23.20.Lv, 23.35.+g, 27.60.+j

I. INTRODUCTION

The study of isomeric nuclear states provides information to interpret intrinsic single-particle nuclear configurations. The presence of isomers can result from a multitude of structural effects that lead to a hindrance in the measured transition probabilities when compared with theoretical single-particle estimates [1]. Neutron-deficient rare-earth nuclei have been shown to exhibit a collection of isomeric states. These are established to predominantly result from changes in nuclear deformations between different quasiparticle configurations: *shape isomers*, as well as the hindrances related to large variations in the total angular momentum projections of axially symmetric deformed states: *K isomers*. In particular, the midshell $N = 74$ isotones provide several examples of long-lived K isomers. Systematic studies of the isotones, ^{132}Ce [2,3], ^{134}Nd [4], ^{136}Sm [5,6], ^{138}Gd [7,8], and ^{140}Dy [9,10] have assigned low-lying isomeric states to two-quasineutron $[514]9/2^- \otimes [404]7/2^+$ configurations with an angular momentum projection of $K^\pi = 8^-$. These isomeric states are observed to decay back to the ground-state rotational bands at a rotational frequency in the region of the first $h_{11/2}$ proton alignment [11]. These band crossings result in the introduction of admixtures of nonzero K values into the ground-state sequence to the extent that in ^{138}Gd the 8^+ member of the ground-state band is calculated to consist of approximately 8% of the $K = 8$ configuration [7]. Such band mixing is one explanation behind the trend in measured hindrances per degree of K forbiddenness observed across the $N = 74$ isotones, where the reduced hindrance is established to decrease with increasing mass. Another possible contribution to the isomer hindrance lies in the change in shape between the isomeric and ground-state structures and the effect of triaxial degrees of freedom. For instance, a second, fragmented decay path out of the 8^- isomeric state was recently identified in ^{132}Ce [3]. The $K^\pi = 8^-$ isomer was deduced to have an element of triaxial deformation and an appreciable amount of γ softness.

The identification of the underlying single-particle configuration of isomeric states, such as those identified in the neutron-deficient $N = 74$ isotones, usually requires an understanding of the γ-ray transitions that feed the isomeric state. The measurement of γ-ray intensity branching ratios $I(M1)/I(E2)$ above an isomeric state allows a comparison to be made between experimental and theoretical g factors for all of the possible quasiparticle configurations around the Fermi surface. However, strongly coupled bands above isomeric states are often weakly populated because they are nonyrast. This can make it difficult to isolate them from the vast number of decays associated with fusion-evaporation reactions. The work presented in this paper has utilized the recoil-isomer tagging technique, which has proven successful in analyzing states built upon isomeric configurations in nuclei in the rare-earth area of the nuclear chart [8,12–16]. This technique was first used in ^{138}Gd to correlate prompt and delayed transitions across a 6-μs isomeric state [7,8]. The high selectivity and sensitivity of this method allowed the weakest of transitions associated with a $K^\pi = 8^-$ isomer to be identified in the prompt spectra. In addition, higher-lying

*On Leave at Department of Physics, University of Jyväskylä, FIN-40014 Jyväskylä, Finland.

†Present address: Department of Physics, University of Surrey, Guildford GU2 5XH, United Kingdom.

‡Present address: Department of Physics, University of Helsinki, FIN-00014 Helsinki, Finland.

prompt rotational structures were observed and assumed to arise from four-quasiparticle configurations, which fed into the known $K^\pi = 8^-$ isomeric state [8].

In the present experiment, the higher statistics collected have resulted in the extension of the $K^\pi = 8^-$ band and have linked in the higher-lying four-quasiparticle states. The experimentally measured properties of these states, g factors, angular distributions, and aligned angular momenta, have been compared with theoretical potential-energy surface (PES) calculations to assign underlying single-particle configurations to these multiquasiparticle states. The higher-lying four-quasiparticle states do not appear to show any hindrance in the measured transition strengths. This lack of hindrance may suggest that at higher spins, the prolate, near axially symmetric shape associated with the lower-lying $K^\pi = 8^-$ isomeric state is lost. The presence of triaxial deformation makes the assignment of multiquasiparticle states to specific configurations difficult; indeed, different configurations have been assigned to what at first glance appear to be analogous bands across the lower-mass even-even isotones [2,4,6]. The validity of K as a *good* quantum number with triaxially deformed shapes is important to being able to fully understand the structure of multiquasiparticle states. A theoretical framework that encompasses triaxial degrees of freedom is essential to be able to examine these structures. Alternatively, the lack of isomerism for the decay from higher-lying four-quasiparticle structures may also be the result of statistical mixing of states with the same spin and parity [17]. Since these high-spin four-quasiparticle structures lie at high excitation energies, the density of nuclear states is greater than at energies where the two-quasiparticle $K^\pi = 8^-$ states are typically observed. This larger density of states is expected to increase the probability for decay [17].

II. EXPERIMENTAL METHODS AND DATA ANALYSIS

Excited states were populated in ^{138}Gd via the ^{106}Cd(^{36}Ar,$2p2n$)^{138}Gd reaction. The K130 cyclotron at the Accelerator Laboratory of the University of Jyväskylä was used to accelerate an $^{36}Ar^{8+}$ beam at an energy of 180 MeV onto a 1-mg/cm^2 ^{106}Cd foil located at the center of the JUROGAM II γ-ray spectrometer [18]. The beam current averaged $\sim$5 particle-nA (pnA) over an approximate running time of 44 h. A total of 3×10^9 recoil-gated prompt events were recorded, with 1×10^6 prompt events correlated with ^{138}Gd decays at the focal plane. In this reaction, ^{138}Gd was populated with a relative cross section of $\sim$6%, with ^{138}Eu ($\sim$41%),^{137}Sm ($\sim$16%), ^{138}Sm ($\sim$12%), and ^{139}Gd ($\sim$8%) populated to a larger extent.

Prompt decays were detected in the JUROGAM II γ-ray spectrometer, comprising 39 Compton-suppressed germanium detectors (15 EUROGAM Phase 1 type detectors and 24 clover detectors). The total photopeak efficiency of JUROGAM II was 6% at 1332 keV. Recoiling fusion-evaporation residues were separated from beamlike particles by the Recoil Ion Transport Unit (RITU) gas-filled recoil separator [19,20] and were transported to the GREAT focal-plane spectrometer [21]. The GREAT spectrometer comprised a multiwire proportional counter (MWPC) at the entrance to two double-sided silicon strip detectors (DSSDs) [22] into which the recoiling nuclei were implanted. Conditions imposed on the time of flight (TOF) between the MWPC and the DSSD and the measured energy loss in the MWPC provided a method to distinguish the beamlike from targetlike nuclei. The GREAT planar and clover germanium detectors were used to detect delayed γ rays emitted after implantation. The planar strip detector had an absolute efficiency of $\approx$30% at 100 keV [21] and was ideally suited to the detection of low-energy γ-ray transitions from isomeric states.

Events were time stamped by a 100-MHz clock through the triggerless total data readout (TDR) acquisition system [23]. Data were collected for off-line sorting with the GRAIN software package [24]. The data were sorted into two-dimensional spectra (matrices) and three-dimensional spectra (cubes) for analysis with the UPAK [25] and RADWARE [26] software suites, respectively. A two-dimensional, asymmetric matrix of prompt γ-ray transitions against correlated delayed γ rays was initially constructed. The prompt decays were correlated with both a recoil implantation in the DSSD and a γ ray detected in either the focal planar or clover detectors of GREAT within 20 μs after a recoil implantation. This time condition was based upon the prior knowledge of the half-life of the isomeric state in ^{138}Gd, measured to be 6(1) μs [7]. The matrix was background subtracted in time, using the period 0–20 μs prior to the arrival of an event in the DSSD to remove any contamination from γ-ray transitions depopulating longer-lived isomeric states or β decays from previously implanted recoils.

Angular distributions were measured for several of the new γ-ray transitions in ^{138}Gd identified in this work. This was achieved by sorting the recoil-isomer-tagged data into the four separate rings of the JUROGAM II spectrometer. The measured intensities at each angle θ, with respect to the beam axis, were fitted with Legendre polynomials of the form

$$W(\theta) = A_0 + A_2 P_2 \cos(\theta) + A_4 P_4 \cos(\theta), \qquad (1)$$

adopting the formalism outlined by Yamazaki [27]. Theoretically calculated distributions were compared with the experimental data points in order to determine the value of the A_2 coefficient. The inclusion of the A_4 coefficient in the theoretical $\Delta I = 1$ distributions was used to reveal the presence of any quadrupole mixing through the observation of the mixing-ratio parameter δ. However, the limited number of JUROGAM II detector rings only allowed the sign of δ to be determined and not its absolute value.

III. RESULTS

A previous study of states built above the $K^\pi = 8^-$ isomer in ^{138}Gd by Cullen *et al.* [8] was able to establish the sequence of γ rays up to the 12^- state in band 1. However, due to low statistics, assignments were based upon consideration of energy sums, intensities, and branching ratios. That work was also able to tentatively identify transitions that appeared to belong to higher-lying rotational bands in ^{138}Gd from comparisons with the lower-mass even-even nuclei. However, without coincidence analysis, these transitions, assigned to ^{138}Gd, were not able to be placed in the decay scheme.

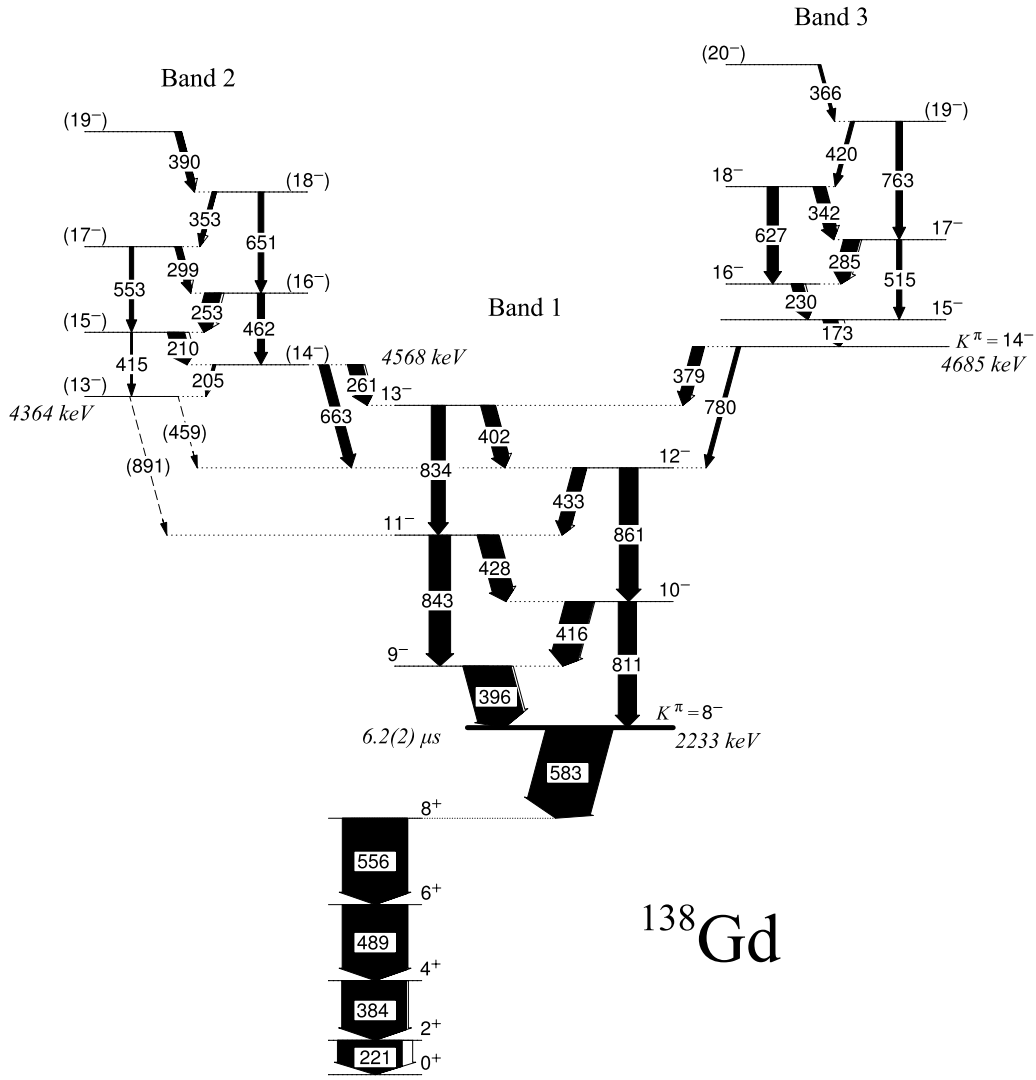

FIG. 1. Partial level scheme of states above and below the $K^\pi = 8^-$ isomer in ^{138}Gd, showing the four-quasiparticle bands identified from recoil-isomer tagging in the present work. The widths of the arrows are proportional to the intensity of the transition, with the white component of each arrow indicating the calculated internal conversion component.

The new ^{138}Gd level scheme deduced in this work is shown in Fig. 1. For simplicity, only the ground-state band sequence up to the 8^- isomer has been included. (The full level scheme of ^{138}Gd can be found in Ref. [11].) The new level scheme above the $K^\pi = 8^-$ isomeric state has been considerably extended in excitation energy and spin from the previous work [8], with the identification of two new (higher-K) four-quasiparticle bands that have been linked into the known $K^\pi = 8^-$ band 1. Table I contains the spectroscopic information for all of the γ rays established in this work. Following the recoil-isomer tagging method outlined in Ref. [8], a series of gated matrices were constructed for analysis. Gating on the energies of known delayed transitions depopulating the $K^\pi = 8^-$ isomer allowed the observation of the correlated prompt decays above the isomeric state. A sum of prompt spectra gated on all five delayed ground-state band transitions (221-, 384-, 489-, 556-. and 583 keV) is shown in Fig. 2(a), and the delayed spectrum resulting from a sum of gates on the known prompt transitions (396-, 416-, 428-, 433-. and 402 keV) is shown in Fig. 2(b). The high level of statistics observed in the isomer-tagged prompt spectra allowed the construction of a recoil-isomer-tagged prompt γ-γ coincidence matrix, where only prompt coincident γ rays associated with a delayed isomeric transition were included. Finally, in order to fully examine the structure of decays depopulating the isomeric state, a delayed γ-γ matrix was constructed from delayed transitions observed in both the planar and clover detectors combined.

Figure 3 shows a set of prompt spectra obtained from setting gates in the recoil-isomer-tagged prompt-prompt γ-γ matrix. Figure 3(a) shows the spectrum resulting from a single gate on the prompt 396-keV transition feeding the $K^\pi = 8^-$ isomer in band 1. The nonobservation of the 811-keV peak, as observed in the total projection in Fig. 2(a), confirms the placement of the 811-keV transition to be parallel to the 396-keV γ ray. The higher-lying transitions observed in the previous study [8] can all be seen, including several previously unidentified transitions. The $K^\pi = 8^-$ band 1 has been extended from the previous work by the addition of the 402- and 834-keV γ rays. These were placed at the top of the band based upon

TABLE I. Prompt γ-ray energies, intensities, initial and final spins, angular distribution coefficients, and mixing ratio signs for transitions above the $K^\pi = 8^-$ isomer in ^{138}Gd deduced in this work. The errors associated with the energies and intensities have been calculated from the spread of their distribution observed in a series of spectra gated on various delayed transitions.

E_γ (keV)	I_γ	$J_i^\pi \rightarrow J_f^\pi$	A_2	A_4	signδ	σL
172.5(2)	30(1)	$15^- \rightarrow 14^-$	−0.21(7)	0.02(1)	+	$M1/E2$
204.6(3)	<5	$(14^-) \rightarrow (13^-)$				$(M1)$
209.6(2)	33(3)	$(15^-) \rightarrow (14^-)$	−0.28(7)	0.01(1)	−	$M1/E2$
230.2(2)	21(2)	$16^- \rightarrow 15^-$	−0.15(8)	0.02(2)	+	$M1/E2$
253.3(2)	31(3)	$(16^-) \rightarrow (15^-)$	−0.35(7)	0.02(1)	−	$M1/E2$
261.3(3)	32(1)	$(14^-) \rightarrow 13^-$	−0.55(15)	0.01(1)	−	$M1/E2$
285.1(2)	34(3)	$17^- \rightarrow 16^-$	−0.13(4)	0.01(1)	+	$M1/E2$
299.1(4)	15(3)	$(17^-) \rightarrow (16^-)$	$-0.28^{+0.04}_{-0.07}$	0.01(1)	−	$M1/E2$
342.2(2)	27(3)	$18^- \rightarrow 17^-$	−0.15(4)	0.00(1)	+	$M1/E2$
352.9(2)	10(3)	$(18^-) \rightarrow (17^-)$	−0.30(7)	0.02(1)	+	$M1/E2$
366.1(8)	6(1)	$(20^-) \rightarrow (19^-)$				$(M1)$
378.9(3)	22(4)	$14^- \rightarrow 13^-$	−0.49(7)	0.01(1)	−	$M1/E2$
389.9(7)	12(2)	$(19^-) \rightarrow (18^-)$				$(M1)$
395.8(2)	100(2)	$9^- \rightarrow 8^-$	−0.66(6)	0.02(1)	−	$M1/E2$
402.2(2)	31(3)	$13^- \rightarrow 12^-$	−0.71(1)	0.03(1)	−	$M1/E2$
414.9(9)	3(2)	$(15^-) \rightarrow (13^-)$				$(E2)$
416.2(3)	57(5)	$10^- \rightarrow 9^-$	−0.56(10)	0.01(2)	−	$M1/E2$
420.4(6)	10(2)	$(19^-) \rightarrow 18^-$				$(M1)$
428.1(2)	48(6)	$11^- \rightarrow 10^-$	−0.72(10)	0.03(1)	−	$M1/E2$
433.0(2)	28(4)	$12^- \rightarrow 11^-$	−0.61(10)	$0.02^{+0.03}_{-0.01}$	−	$M1/E2$
458.6(7)	< 4	$(13^-) \rightarrow 12^-$				$(M1)$
462.4(2)	9(6)	$(16^-) \rightarrow (14^-)$				$(E2)$
514.6(12)	11(3)	$17^- \rightarrow 15^-$				$(E2)$
552.8(13)	11(3)	$(17^-) \rightarrow (15^-)$				$(E2)$
626.8(8)	26(3)	$18^- \rightarrow 16^-$				$(E2)$
651.2(9)	12(2)	$(18^-) \rightarrow (16^-)$				$(E2)$
663.0(11)	21(3)	$(14^-) \rightarrow 12^-$	0.38(3)	−0.13(2)		$E2$
762.6(8)	13(5)	$(19^-) \rightarrow 17^-$				$(E2)$
780.0(10)	9(4)	$14^- \rightarrow 12^-$				$(E2)$
811.1(3)	35(4)	$10^- \rightarrow 8^-$	0.28(3)	−0.05(2)		$E2$
834.0(2)	32(5)	$13^- \rightarrow 11^-$	0.15(3)	−0.01(1)		$E2$
842.7(4)	48(3)	$11^- \rightarrow 9^-$	$0.18^{+0.13}_{-0.07}$	$-0.02^{+0.01}_{-0.05}$		$E2$
860.8(4)	41(3)	$12^- \rightarrow 10^-$	$0.12^{+0.11}_{-0.08}$	$-0.03^{+0.01}_{-0.04}$		$E2$
891.4(7)	<3	$(13^-) \rightarrow 11^-$				$(E2)$

coincidence analysis as well as energy sums and intensity considerations. Angular distribution measurements confirm the tentative dipole and quadrupole assignments proposed in the previous work as well as the new transitions established in this work (see Table I). Figure 4 shows the angular distribution measurements for four of the γ-ray transitions in band 1. A negative sign for the dipole-quadrupole mixing ratio δ in band 1 was deduced from the comparison of theoretical distributions [27] with the experimental data points, with the inclusion of the A_4 coefficient in the angular distribution fit. The sign of the mixing ratio measured in this work is consistent with that assumed for states above the $K^\pi = 8^-$ isomer in ^{136}Sm [6].

Figure 3(b) shows a spectrum gated on the prompt 261-keV transition that links band 2 to band 1. The 663-keV γ-ray observed in Fig. 3(a) is not present in Fig. 3(b), which suggests that it belongs to a parallel cascade. The intense $\Delta I = 1$ transitions assigned to this band are clearly seen at low energy; however, the weaker quadrupole crossover γ rays are difficult to distinguish from the background. They were established to be part of band 2 because they were observed in summed spectra, gated on all of the interband mixed dipole-quadrupole transitions. Angular-distribution measurements performed for the more intense transitions in band 2 (210-, 253-, 299-, and 353-keV) resulted in mixed dipole-quadrupole assignments. The potential quadrupole mixing into the $\Delta I = 1$ transitions was evaluated by comparing the experimental data points with theoretical distributions that included the A_4 coefficient. From this comparison it was possible to establish a small negative mixing ratio for each of the measured transitions.

Figure 3(c) shows the prompt spectrum resulting from a single gate set on the 253-keV γ ray in band 2. The two transitions linking bands 1 and 2 via the 261- and 663-keV γ rays are both evident in this spectrum, consistent with the placement of the band. The majority of the intensity flow from band 2 to band 1 is established to pass through the 663- and 261-keV γ rays. However, the presence of the (13^-) state in band 2 suggests that band 2 also feeds into band 1 at lower

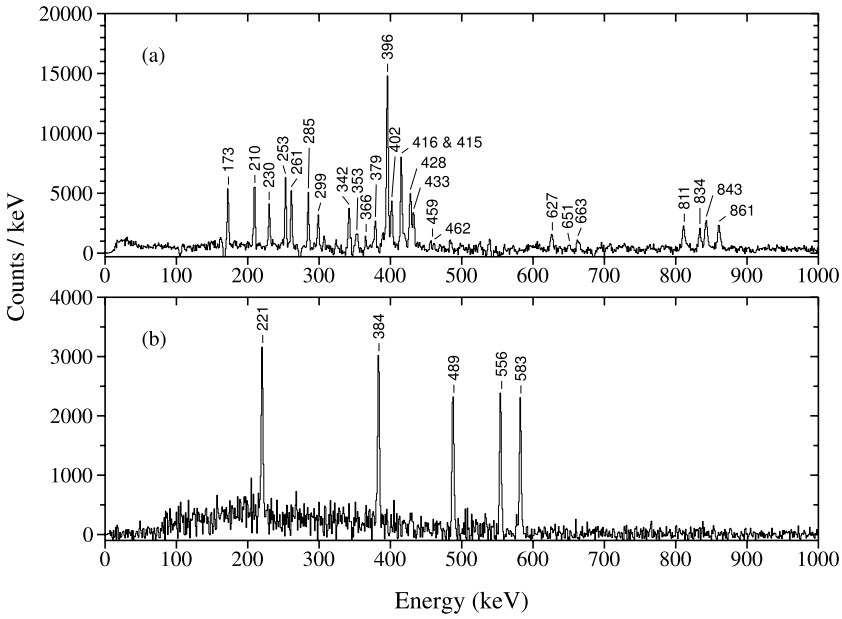

FIG. 2. (a) Sum spectrum of prompt γ-ray transitions in the JUROGAM II spectrometer obtained by gating on the 221-, 384-, 489-, 556-, and 583-keV delayed transitions in ^{138}Gd. The spectrum was also gated by the region of time from 0 to 20 μs after a recoiling nucleus implanted into the DSSD. A background time subtraction was performed for the interval 0–20 μs prior to this implantation. (b) Sum spectrum of delayed transitions obtained by gating on the 396-, 416-, 428-, 433-, and 402-keV prompt transitions in the $K^\pi = 8^-$ band, with the same time conditions as Fig. 2(a).

spins. The tentatively placed 891- and 459-keV transitions, which are thought to feed into band 1 at lower spins, are not evident in this particular spectrum. In addition, the ratio of the intensities of the 416- and 428-keV transitions in band 1 in Fig. 3(c), gated on the 253-keV γ ray, differs from that shown in Fig. 3(b), gated on the 261-keV transition. The larger intensity observed in the 416-keV peak in Fig. 3(c) highlights the doublet nature of the 416-keV γ ray, which has been assigned in this work to bypass the 14^- in-band state in band 2.

Figure 3(d) shows a prompt spectrum from a gate set on the 173-keV transition assigned to band 3. None of the transitions assigned to band 2 are visible in the spectrum, confirming that bands 2 and 3 are two separate higher-lying bands. The $E2$ crossover transitions in band 3 are hard to distinguish from the background because of the reduced detector efficiency at higher energies compared with lower energies, where the intense $\Delta I = 1$ transitions are clearly observed in this spectrum. Angular distribution measurements confirmed the mixed dipole-quadrupole nature of the 173-, 230-, 285-, and 342-keV transitions within band 3. A small positive mixing ratio was measured for these transitions above the 15^- state in band 3.

The half-life of the isomeric $K^\pi = 8^-$ state was deduced by constructing a matrix of the time between recoil implantation in the DSSD and delayed γ-ray detection in the planar detector against γ-ray energy. By gating on the known delayed transitions in ^{138}Gd and subtracting background from the energy spectra, time projections were produced for each of the five delayed transitions below the isomer. Figure 5 shows the time spectrum from a sum of gates on the 221-, 384-, 489-, 556-, and 583-keV transitions. The measured half-life of 6.2(2) μs was determined from a weighted average of exponential fits to each of the five individual time spectra. This result is consistent with, but more accurate than, the value measured by Bruce *et al.* of 6(1)μs [7].

IV. DISCUSSION

Gadolinium-138 has been extensively researched by several collaborations [7,8,11,28,29]. The study performed by Paul *et al.* [11] was able to establish several prompt bands in ^{138}Gd up to high spin. Comparisons between the experimental alignments and theoretical cranked shell model (CSM) calculations assigned several bands to different multi-quasiparticle configurations. These low-lying configurations are composed of orbitals that lie near the Fermi surface. Combinations of these orbitals may be expected to contribute to the high-spin nonyrast states observed in this work.

PES calculations have been performed for a variety of excited two- and four-quasiparticle configurations based upon combinations of the orbitals observed to reside around the Fermi surface. These calculations were performed using the configuration-constrained blocking method, where specified single-particle orbitals responsible for the observed quasiparticle excitations are kept singly occupied as the deformation is varied [30,31]. In order to identify the specific single-particle orbitals that need to be blocked adiabatically in pairing calculations, a set of average Nilsson numbers, $\langle N\rangle$, $\langle n_z\rangle$, $\langle\Lambda\rangle$, and $\langle|\Omega|\rangle$, were calculated for the required configurations. The PESs, obtained for each rotational frequency, were calculated at quadrupole deformation (β_2, γ) with hexadecapole (β_4) variation. This method has been successful in reproducing experimentally observed excitation energies of quasiparticle configurations for many nuclei in the rare-earth area of the nuclear chart [10,31,32]. Table II summarizes the predicted deformations and excitation energies for a combination of quasiparticle configurations in ^{138}Gd.

In this work, the same method for determining theoretical g factors as Ref. [8] has been employed for the higher-lying four-quasiparticle bands. However, in contrast, in this work, the transition quadrupole moments were determined from

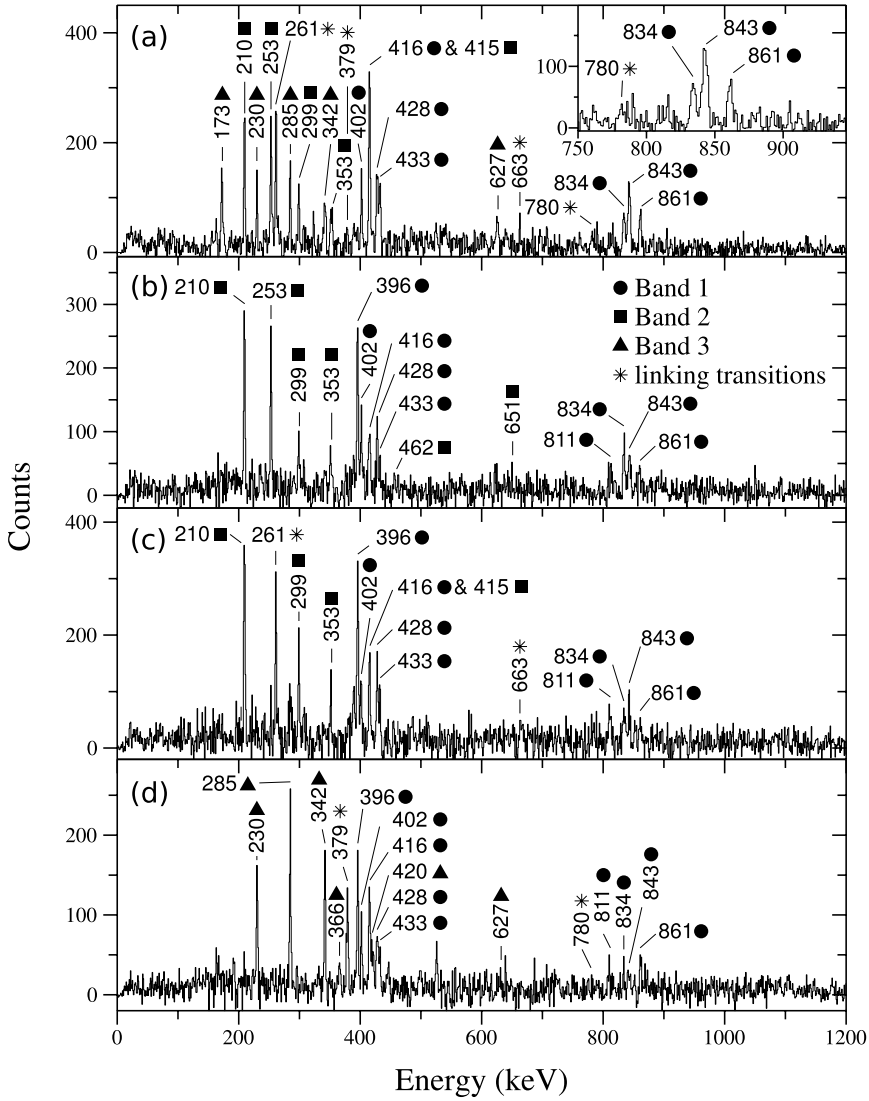

FIG. 3. Prompt γ-γ spectra from a recoil-isomer-tagged matrix of ^{138}Gd recorded with the JUROGAM II array. Only the most prominent γ rays are indicated. (a) A single gate on the 396-keV transition in band 1 and (b) a single gate on the 261-keV transition linking bands 1 and 2. (c) A single gate on the 253-keV transition in band 2 and (d) a single gate on the 173-keV transition in band 3.

Ref. [33]:

$$Q_t = Q_{20} + \sqrt{\frac{2}{3}} Q_{22}, \tag{2}$$

where the components of the quadrupole moment were calculated microscopically from the values of β and γ, derived from the PES calculations. Quadrupole moments derived from this theoretical prescription include triaxial degrees of freedom, which were not incorporated in previous values taken from experimental data [33].

In the following sections, the g factors, configuration-constrained blocking calculations, angular distributions, and alignments will be discussed for each of the four-quasiparticle high-K bands separately. The experimental aligned angular momentum (alignment) i_x [34], as a function of rotational frequency, was determined for each of the high-K bands in ^{138}Gd measured in this work. A reference band with Harris parameters [35] $\Im_0 = 11.0\hbar^2/\text{MeV}$ and $\Im_1 = 25.8\hbar^4/\text{MeV}^3$ was subtracted from each band.

A. $K^\pi = 8^-$ two-quasiparticle configuration

Figure 6 shows the PES predictions for ^{138}Gd following the $K^\pi = 8^-$ configuration through increasing rotational frequencies. These calculations allow the change in nuclear shape to be followed above the band-head state, giving information on the structure of the nucleus all the way up to the point at which higher-lying configurations feed into the band. In each instance the minima are found to be γ-soft (see Fig. 6), implying a high degree of susceptibility to vibrational degrees of freedom. This γ softness may be the reason that the change in $E2$ energies above the 8^- state appear to deviate slightly from that expected for a purely rotational prolate-deformed nuclear shape. In the absence of γ softness the energies of the $E2$-crossover transitions would be expected to increase more rapidly with rotational frequency, as observed in the ground-state band. The energy minimum is seen to evolve from an axially symmetric shape at low rotational frequencies toward a triaxially deformed nuclear shape at $\hbar\omega = 0.15$ MeV. The requirements of the configuration-constrained method limit the calculation of configurations to $|\gamma| < 30^\circ$ [30,31]. As a consequence, any further shape evolution toward a more

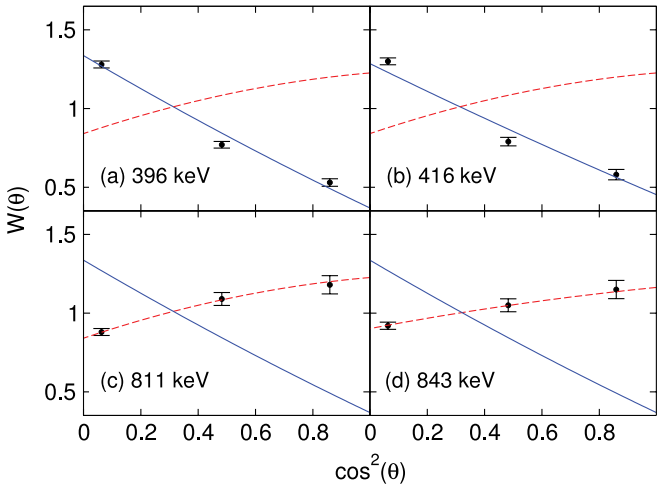

FIG. 4. (Color online) Angular distributions measured for the (a) 396-, (b) 416-, (c) 811-, and (d) 843-keV transitions in band 1 of ^{138}Gd. Dashed lines correspond to an $E2$ (quadrupole) transition, and solid lines correspond to a mixed $M1/E2$ (dipole-quadrupole) transition. A substate population alignment of $\sigma/I = 0.3$ was chosen for the theoretical dipole distributions. This value was deduced from the weighted average of all quadrupole transitions measured in band 1. Data for the two clover rings around 90° to the beam axis have been combined into one $\cos^2(\theta)$ angle.

oblate deformation cannot be followed within the current PES method. In order to establish any effects of this apparent change in shape with increasing spin in the two-quasineutron band, the behavior of higher-lying configurations is discussed in Sec. IV B.

B. Four-quasiparticle configurations

The analysis techniques outlined at the start of Sec. IV have been used to assign configurations to the two new higher-lying four-quasiparticle states. Table II shows the results of PES calculations performed for four-quasiparticle configurations that include the two-quasineutron configuration assigned to the $K^\pi = 8^-$ isomeric state. A combination of four-quasineutron and two-quasineutron plus two-quasiproton configurations are predicted to have excitation energies similar to those observed for bands 2 and 3 measured in this work. Figure 7 shows

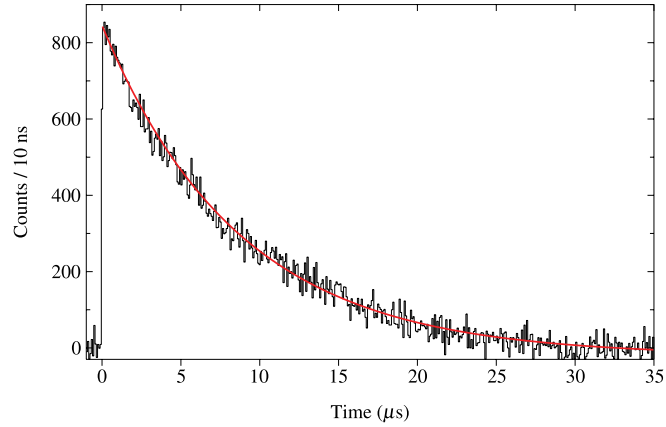

FIG. 5. (Color online) Time spectrum for the 221-, 384-, 489-, 556-, and 583-keV γ-ray transitions in the ground-state band. An exponential fit to the data gives a half-life of 6.2(2) μs. The time axis defines the time difference between a recoil implantation in the GREAT DSSD and a γ-ray detection in the GREAT planar detector.

the experimental g factors, including the weighted average values for each band (dashed lines) and the theoretical g factors (solid lines) based upon Nilsson orbitals shown in Table II. The g factors were determined from a rotational model of the nucleus, which includes a theoretically determined value of the dipole-quadrupole mixing ratio δ. This is consistent with the method used to determine the g factors for the $K^\pi = 8^-$ band in Ref. [8].

1. Band 2

Band 2 has been tentatively assigned to the $K^\pi = 12^-$, $\nu\{9/2^-[514]7/2^+[404]\} \otimes \pi\{3/2^+[411]5/2^+[413]\}$ configuration. The experimental g factors for band 2, assuming a value of K of 12, were not definitive in their contribution to the configuration assignment to the band-head state. A negative value was adopted for the g factors based upon the negative mixing ratio observed in the angular distribution fits of the mixed $M1/E2$ transitions in band 2 [6]. Although the band-head excitation energy is consistent with that theoretically predicted for four-quasiparticle configurations, higher statistics are required to better determine the g factors for

TABLE II. Deformations, excitation energies, and g factors calculated with the configuration-constrained blocking method for a combination of both two- and four-quasiparticle configurations based on nuclear orbitals around the Fermi surface in ^{138}Gd. Q_t was determined from Eq. (2) in the calculation of the theoretical g factors.

I^π	E_{calc} (keV)	E_{exp} (keV)	Configuration	$(g_k - g_R)$ $[\mu_N]$	β_2	$\lvert\gamma\rvert$ (deg)	β_4
8^-	2100	2233	$\nu\{9/2^-[514] \otimes 7/2^+[404]\}$	−0.46	0.25	10 (soft)	−0.031
11^-	4324		$\nu\{9/2^-[514]7/2^+[404] \otimes 5/2^+[402]1/2^+[400]\}$	−0.67	0.24	8	−0.033
12^-	4871		$\nu\{9/2^-[514]7/2^+[404] \otimes 7/2^-[523]1/2^-[541]\}$	−0.66	0.26	8	−0.010
12^-	4654		$\nu\{9/2^-[514]7/2^+[404]\} \otimes \pi\{3/2^+[411]5/2^+[413]\}$	−0.13	0.26	2	−0.017
14^-	4829	4685	$\nu\{9/2^-[514]7/2^+[404]\} \otimes \pi\{5/2^-[532]7/2^-[523]\}$	0.13	0.25	9 (soft)	−0.033
12^+	4493		$\nu\{9/2^-[514]7/2^+[404]\} \otimes \pi\{5/2^-[532]3/2^+[411]\}$	0.07	0.25	0 (soft)	−0.029
14^+	4747		$\nu\{9/2^-[514]7/2^+[404]\} \otimes \pi\{5/2^+[413]7/2^-[523]\}$	−0.04	0.25	10 (soft)	−0.031

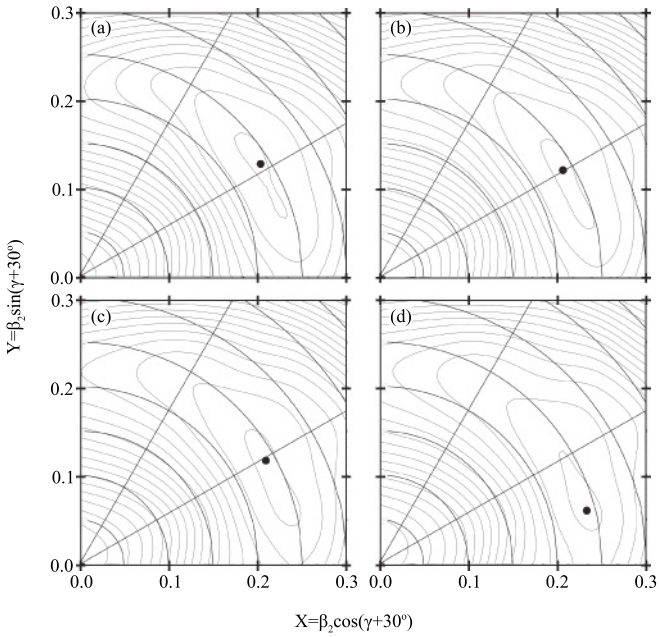

FIG. 6. Calculated PESs following the $K^\pi = 8^-$ two-quasineutron $\nu\{9/2^-[514] \otimes 7/2^+[404]\}$ configuration in ^{138}Gd for increasing rotational frequency. The panels correspond to frequencies $\hbar\omega$ of (a) 0, (b) 0.05, (c) 0.10, and (d) 0.15 MeV. The evolution of the absolute minimum with rotational frequency from a prolate to a more triaxial nuclear shape is evident.

this band. The g factor measurements made in this work, however, tend to favor a quasiproton pair for the observed band structure because the theoretically predicted configurations involving only neutrons have much larger negative g factors. This $\{3/2^+[411]5/2^+[413]\}$ quasi-proton alignment may be expected, as the neutron crossings are not predicted to occur until higher rotational frequencies [11]. The two aligned quasiprotons, thought to make up the four-quasiparticle band-head state in band 2, belong to the $\pi 2d_{5/2}$ and $\pi 1g_{7/2}$ orbits, respectively. Protons from these two orbits are predicted to contribute to the first observed alignment in the ground-state configuration of ^{138}Gd [11], where CSM calculations reveal these orbitals to become yrast at frequencies of $\hbar\omega \approx 3.5$ MeV. This may explain why the $I^\pi = 14^-$ state of band 2 occurs at a slightly lower excitation energy than that of band 3 (see Fig. 1). Angular distribution measurements appear to favor an $I^\pi = 14^-$ assignment for the apparent band-head state of band 2. This does not correlate well with the predicted $K^\pi = 12^-$ configuration from the PES calculations, which has a better match between experimental and theoretical g factors and excitation energies. In the current work, only four detector rings were available for fitting angular distributions to, and it cannot be fully ruled out that neither the 663- nor the 261-keV transitions are fully stretched. In this instance the lower-lying (13^-) state may well have $I^\pi = 12^-$. However, at a lower excitation energy, the correspondence between this energy and that predicted theoretically is less revealing. For these reasons, the 12^- configuration has only been tentatively assigned to the four-quasiparticle configuration of band 2.

2. *Band 3*

Band 3 has been assigned to the $K^\pi = 14^-$, $\nu\{9/2^-[514]7/2^+[404]\} \otimes \pi\{5/2^-[532]7/2^-[523]\}$ configuration. This assignment was based upon the comparison of several experimental features with the corresponding theoretical predictions. The experimental g factors measured for band 3, assuming a value of K of 14, are in good agreement with those predicted for the two-quasineutron plus two-quasiproton configuration, which incorporates the two-quasineutron configuration assigned to the $K^\pi = 8^-$ band 1 (see Fig. 7). A positive value for the experimental g factors for this band was based upon the positive mixing ratio measured for the $\Delta I = 1$ transitions, combined with the theoretically predicted positive value for Q_t [6]. Angular distribution measurements for the 379-keV transition suggest a band-head state with a spin and parity of 14^-. This is in agreement with the K^π value of 14^- Nilsson-orbital configuration assigned to the band. The

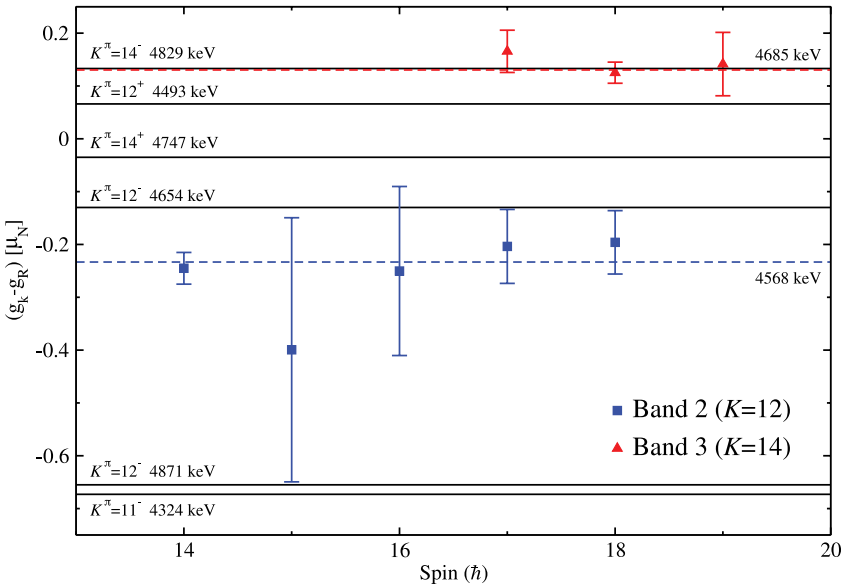

FIG. 7. (Color online) Experimental g factors determined for bands 2 and 3 in ^{138}Gd and theoretical values determined from the PES calculations. The dashed lines show the weighted average experimental value for each band, and the solid lines show the theoretical g factors determined for each of the different theoretical four-quasiparticle configurations. The values of K assumed in the experimental data points are shown in the legend. The experimental (right) and theoretical (left) excitation energies are shown beside each plot.

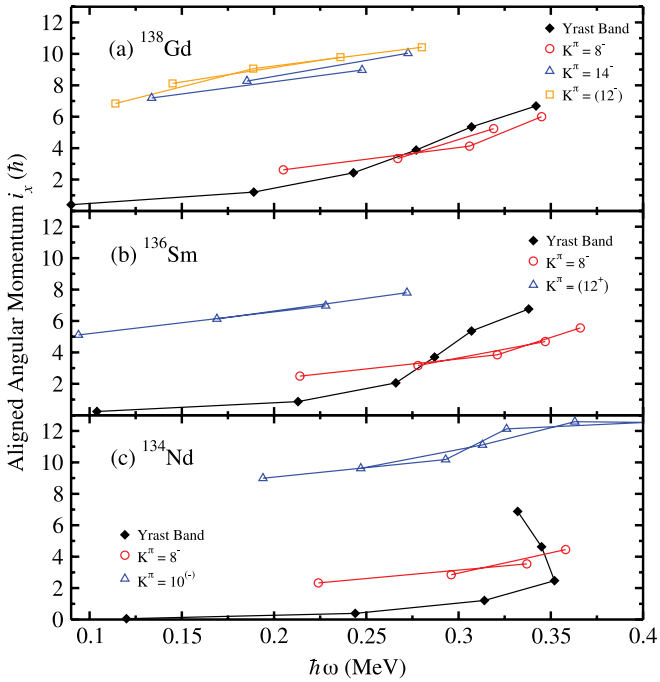

FIG. 8. (Color online) Alignment plots for the ground state, yrast band, $K^\pi = 8^-$ bands, and higher-lying bands in the $N = 74$ isotones ^{138}Gd, ^{136}Sm [6], and ^{134}Nd [4]. The alignments were calculated using the Harris reference parameters $\Im_0 = 11.0\hbar^2/\text{MeV}$ and $\Im_1 = 25.8\hbar^4/\text{MeV}^3$. The values of K for the higher-lying bands in ^{136}Sm and ^{134}Nd were taken from Table III.

theoretically predicted excitation energy of this configuration is 4829 keV and is quite close to the value of 4685 keV measured experimentally. This difference of less than 150 keV in the excitation energies of the band-head state in band 3 is within the accuracy expected for theoretically predicted excitation energies of multiquasiparticle configurations [31]. The alignment plots for band 3 (see Fig. 8) show an initial alignment of $\approx 7\hbar$ at $\hbar\omega = 0.13$ MeV, about $4\hbar$ higher than the initial alignment observed in the two-quasiparticle $K^\pi = 8^-$ band 1. This increase in alignment can be entirely associated with the additional two-quasiprotons in $h_{11/2}$ orbitals. This alignment is slightly smaller than that established in the yrast, ground-state band at $\approx\hbar\omega = 0.3$ MeV, which has been attributed to the alignment of a quasiproton from the $h_{11/2}$ orbit and one of either the $g_{7/2}$ or $d_{5/2}$ orbits [11]. For an $I^\pi = 14^-$ state, the smaller values of Ω associated with orbitals from the $\pi g_{7/2}$ or $\pi d_{5/2}$ orbits would produce too high an initial alignment for band 3. The smaller alignment can then be understood by the inclusion of higher-Ω states from the $\pi h_{11/2}$ orbit. The theoretically predicted γ deformation of $|\gamma| = 9^\circ$ for this configuration (see Table II) may provide a possible explanation for the lack of any hindrance in the decay from band 3 to the $K^\pi = 8^-$ band 1, which is also shown to contain a large degree of γ deformation for increasing rotational frequencies; see Fig. 6.

Similar four-quasiparticle bands have been observed in several of the lower-mass even-even isotones [2,4,6]. The assignments made to these bands were based mainly upon comparisons of experimental branching ratios with predictions made by theory. Table III summarizes the quasiparticle configurations assigned to these structures. In Table III, only high-spin bands whose configurations include that of the two-quasineutron $K^\pi = 8^-$ configuration have been compared. The experimental excitation energies established across these isotones all appear to be consistent with the range of values predicted by the PES for ^{138}Gd in this work. Samarium-136 is the only nucleus where it has been suggested that the high-K band has a four-quasineutron configuration [6]. This was reasoned by the apparently small initial alignment of the band, which should have been larger if there was any contribution from a two-quasiproton pair [6] (see Fig. 8). It can also be seen from Table III that the excitation energy of the four-quasiparticle band head in ^{136}Sm is slightly lower than that seen in the lower-mass isotones, although the transitions linking this band to the 8^- configuration were only tentatively assigned [6].

C. Hindrance factors for two- and four-quasiparticle states

An extensive study by Bruce *et al.* examined the systematic trend in decay hindrances observed in the decay from the $K^\pi = 8^-$ two-quasineutron configurations to the ground-state bands in several of the even-even $N = 74$ isotones [7]. The trend in reduced hindrances for these decays appeared to behave in an opposing manner, as a function of mass, to that expected, where the increase in Z, and consequently the increase in the deformation of the ground-state band, would be expected to stabilize the K selection rule, resulting in larger hindrances for the heavier nuclei [7]. A simple two-band mixing prescription between the ground and s bands was successful in replicating the experimental data. This theoretical framework examined the mixing of higher-K

TABLE III. Four-quasiparticle assignments and experimental excitation energies for the high-K bands in the $N = 74$ isotones ^{138}Gd, ^{136}Sm [6], ^{134}Nd [4], and ^{132}Ce [2]. Only bands that have been assigned to include the $\nu\{9/2^-[514] \otimes 7/2^+[404]\}$ configuration have been included.

Nucleus	Excitation energy (keV)	Four-quasiparticle configurations	K^π
^{138}Gd band 2	4568	$\nu\{9/2^-[514]7/2^+[404]\} \otimes \pi\{3/2^+[411]5/2^+[413]\}$	12^-
^{138}Gd band 3	4829	$\nu\{9/2^-[514]7/2^+[404]\} \otimes \pi\{5/2^-[532]7/2^-[523]\}$	14^-
^{136}Sm	4169	$\nu\{9/2^-[514]7/2^+[404]\} \otimes \nu\{1/2^+[400]7/2^-[523]\}$	12^+
^{134}Nd	4986	$\nu\{9/2^-[514]7/2^+[404]\} \otimes \pi\{1/2^-[550]3/2^-[541]\}$	10^-
^{132}Ce	5638	$\nu\{9/2^-[514]7/2^+[404]\} \otimes \pi(h_{11/2})^2$	...

TABLE IV. Calculated deformations of the two-quasineutron $K^\pi = 8^-$ isomeric band-head states for the $N = 74$ isotones. The corresponding quadrupole moments were derived from Eq. (2) [33].

Nuclei	β_2	$\lvert\gamma\rvert$ (deg)	Q_t (e b)
^{138}Gd	0.250	10	5.11
^{136}Sm	0.228	12	4.48
^{134}Nd	0.215	7	4.33
^{132}Ce	0.195	0	3.83

components into the ground-state band in the crossing region, but several assumptions were required to be included in the analysis. The theoretical PES calculations performed in the present work shed light on the possible contribution to this observed trend from shape-changing effects between the two-quasiparticle isomeric configuration and the ground-state band.

Table II shows the theoretically predicted γ deformation, $|\gamma| = 10^\circ$, and quadrupole deformation, $\beta_2 = 0.25$, for the $K^\pi = 8^-$ configuration in ^{138}Gd. PES calculations performed for increasing rotational frequency in the ground-state band reveal absolute minimums of $\gamma = -13^\circ$ and $\beta_2 = 0.26$ at $\hbar\omega = 0.28$ MeV, corresponding to the $I^\pi = 8^+$ level in ^{138}Gd. In this scenario, it is observed that the two-quasiparticle isomeric state decays into the ground-state band, which has similar values of γ deformation. This extra element of a substantial degree of triaxial deformation common to both structures and the mixing of high-K components in the ground-state band are all expected to counteract the K selection rule, reducing the expected hindrance of the decay from the isomeric state.

Although PES calculations have not been performed for the ground-state sequences in the lower-mass isotones in this work, previous calculations performed for ^{136}Sm [36], ^{134}Nd [37], and ^{132}Ce [2] show the ground-state bands in each nucleus have a considerable amount of γ deformation, around $|\gamma| \approx 15^\circ$, at $\hbar\omega \approx 0.3$ MeV. The effect of this susceptibility to γ vibrations is clearly established in ^{132}Ce, where recent measurements show the decay out of the $K^\pi = 8^-$ state fragmenting into a γ-vibrational band parallel to the ground-state band [3]. Table IV shows the decreasing trend in γ deformation predicted from the PES calculations for the lower-mass $K^\pi = 8^-$ isomeric states. The theoretically predicted values for the isomeric state suggest that the commonality in triaxiality between the two bands may be lost with decreasing mass. As a result, it may be expected that the reduced hindrance could increase with decreasing Z. Further theoretical calculations for all the $N = 74$ isotones would be helpful to fully explore the contribution of triaxial deformation to the hindrances observed in these isomeric states.

The higher-lying four-quasiparticle structures observed in this work for ^{138}Gd have been predicted to contain degrees of γ deformation similar to those of the two-quasiparticle $K^\pi = 8^-$ configuration. It would therefore be expected that any hindrances observed in the decay of these higher structures may be suppressed by the triaxial deformation of the two bands, in a similar way to that outlined above for the $K^\pi = 8^-$ decay to the ground-state band. Combining this with the smaller change in K compared to that between the $K^\pi = 8^-$ isomer and the ground-state band provides a possible explanation for the nonobservation of any hindrance in decays out of these states. However, for these higher-lying states, it is also possible that the increased density of nuclear states with excitation energy plays a role in the reduced hindrances seen from the higher-lying four-quasiparticle states [17]. Theoretical calculations based upon a statistical density of states formulation on reduced hindrances in the $A = 180$ region of the nuclear chart by Walker *et al*. [17] managed to partly reproduce the experimentally observed systematic behavior of the reduced hindrances seen in several of the hafnium and tungsten isotopes. Such effects may well play a similar role in the $A \approx 130$ region of the nuclear chart for these high-K four-quasiparticle configurations.

V. CONCLUSIONS

In conclusion, recoil-isomer tagging has been used in conjunction with the JUROGAM II–RITU–GREAT detector arrangement at the University of Jyväskylä in order to study the states above a known $K^\pi = 8^-$ isomer in ^{138}Gd. Two high-K four-quasiparticle bands have been established and compared to theoretical PES calculations to assign specific Nilsson-orbital configurations. Angular distribution measurements and γ-γ coincidence analysis have confirmed the ordering of previously identified transitions in the two-quasiparticle band as well as those in the newly established high-K bands. Experimental g factors have been calculated based upon intensity branching ratios, which have been used to further confirm the single-particle configurations assigned to the high-spin bands. PES calculations for varying rotational frequencies above the $K^\pi = 8^-$ band-head state reveal a trend toward a more triaxially deformed nuclear shape. This, in combination with the higher level density at high excitation energies, may explain the lack of hindrance observed in the decays of the higher-lying four-quasiparticle configurations.

ACKNOWLEDGMENTS

Useful discussions with Alick Deacon are greatly appreciated. This work has been supported by the EU 6th Framework Programme, "Integrating Infrastructure Initiative Transnational Access," Contract No. 506065 (EURONS), and by the Academy of Finland under the Finnish Centre of Excellence Programme 2006-2011 (Nuclear and Accelerator Based Physics Programme at JYFL). The authors acknowledge the support of the EPSRC/IN2P3 LOANPOOL and European Gammapool owners for the loan of the JUROGAM II detectors. M.G.P acknowledges support by the STFC. D.M.C. acknowledges the support of the STFC through Contract No. PP/F000855/1. P.N and P.T.G. acknowledge the support of the Academy of Finland through Contracts No. 121110 and No. 119290, respectively.

[1] P. Walker and G. Dracoulis, Nature (London) **399**, 35 (1999).
[2] E. S. Paul *et al.* Nucl. Phys. **619**, 177 (1997).
[3] T. Morek *et al.* Phys. Rev. C **63**, 034302 (2001).
[4] C. M. Petrache *et al.* Nucl. Phys. A **617**, 249 (1997).
[5] A. M. Bruce, P. M. Walker, P. H. Regan, G. D. Dracoulis, A. P. Byrne, T. Kibèdi, G. J. Lane, and K. C. Yeung, Phys. Rev. C **50**, 480 (1994).
[6] P. H. Regan, G. D. Dracoulis, A. P. Byrne, G. J. Lane, T. Kibédi, P. M. Walker, and A. M. Bruce, Phys. Rev. C **51**, 1745 (1995).
[7] M. Leino *et al.*, Nucl. Instrum. Methods Phys. Res., Sect. B **99**, 1 (1995).
[8] D. M. Cullen *et al.*, Phys. Rev. C **58**, 846 (1998).
[9] W. Królas *et al.*, Phys. Rev. C **65**, 031303 (2002).
[10] D. M. Cullen *et al.*, Phys. Lett. B **529**, 42 (2002).
[11] E. S. Paul *et al.*, J. Phys. G **20**, 751 (1994).
[12] P. J. R. Mason *et al.*, Phys. Rev. C **81**, 024302 (2010).
[13] P. J. R. Mason *et al.*, Phys. Rev. C **79**, 024318 (2009).
[14] D. M. Cullen *et al.*, Phys. Rev. C **80**, 024303 (2009).
[15] S. V. Rigby *et al.*, Phys. Rev. C **78**, 034304 (2008).
[16] D. M. Cullen Phys. Rev. C **66**, 034308 (2002).
[17] P. M. Walker, Phys. Lett. B **408**, 42 (1997).
[18] P. T. Greenlees, AIP Conf. Proc. **764**, 237 (2005).
[19] M. Leino, Nucl. Instrum. Methods Phys. Res., Sect. B **126**, 320 (1997).
[20] M. Leino, Nucl. Instrum. Methods Phys. Res., Sect. B **99**, 653 (1995).
[21] R. D. Page, Nucl. Instrum. Methods Phys. Res., Sect. B **204**, 634 (2003).
[22] P. T. Greenlees, Eur. Phys. J. A **25**, 599 (2005).
[23] I. Lazarus, IEEE Trans. Nucl. Sci. **48**, 567 (2001).
[24] P. Rahkila, Nucl. Instrum. Methods Phys. Res., Sect. A **595**, 637 (2008).
[25] W. T. Milner, UPAK, The Oak Ridge Analysis Package (Oak Ridge National Laboratory, Oak Ridge, TN).
[26] D. C. Radford, Nucl. Instrum. Methods Phys. Res., Sect. A **361**, 297 (1995).
[27] T. Yamazaki, Nucl. Data, Sect. A **3** (1967).
[28] P. J. Bishop, M. J. Godfrey, A. J. Kirwan, P. J. Nolan, D. J. Thornley, J. M. O'Donnel, R. Wadsworth, D. J. G. Love, and L. Goettig, J. Phys. G **14**, 995 (1988).
[29] C. J. Lister *et al.*, Phys. Rev. Lett. **55**, 810 (1985).
[30] F. R. Xu, P. M. Walker, J. A. Sheikh, and R. Wyss, Phys. Lett. B **435**, 257 (1998).
[31] F. R. Xu, P. M. Walker, and R. Wyss, Phys. Rev. C **59**, 731 (1999).
[32] P. Mason, Phys. Lett. B **683**, 17 (2010).
[33] R. W. Laird, Phys. Rev. Lett. **88**, 152501 (2002).
[34] R. Bengtsson and S. Frauendorf, Nucl. Phys. A **314**, 27 (1979).
[35] S. M. Harris, Phys. Rev. **138**, B509 (1965).
[36] E. S. Paul, J. Phys. G **19**, 861 (1993).
[37] T. Klemme, Phys. Rev. C **60**, 034301 (1999).